Mucoadhesive and thermosensitive Bletilla striata polysaccharides/chitosan hydrogel loaded nanoparticles for rectal drug delivery in ulcerative colitis

Shiyi Zhao
Chengdu University of Traditional Chinese Medicine
Junbo Zhang
Chengdu University of Traditional Chinese Medicine
Mengyu Qiu
Chengdu University of Traditional Chinese Medicine
Yusen Hou
Chengdu University of Traditional Chinese Medicine
Xuebo Li
Chengdu University of Traditional Chinese Medicine
Guofeng Zhong
Chengdu University of Traditional Chinese Medicine
Kaijun Gou
Southwest Minzu University
Jingjing Li
Hong Kong Polytechnic University
Chen Zhang
Chengdu University of Traditional Chinese Medicine
Yan Qu
Chengdu University of Traditional Chinese Medicine
Xiao Wang
wangxiao12643@126.com

Southwest Minzu University

Research Article

Keywords: Ulcerative colitis, Thiolated-hyaluronic acid, Thermosensitive hydrogel, Bletilla striata polysaccharides, Puerarin

Posted Date: August 1st, 2023

DOI: https://doi.org/10.21203/rs.3.rs-3205487/v1

Additional Declarations: No competing interests reported.

Version of Record: A version of this preprint was published at International Journal of Biological Macromolecules on January 1st, 2024. See the published version at https://doi.org/10.1016/j.ijbiomac.2023.127761.

Abstract

Ulcerative colitis (UC) is a chronic disease with diffuse mucosal inflammation limited to the colon. A topical drug delivery system that could be facilely performed and efficiently retained at colon are attractive for clinical ulcerative colitistreatment. Herein, a novel platform for rectal administration of thermosensitive hydrogel co-loaded with nanoparticles to treat ulcerative colitis was developed. Thiolated-hyaluronic acid was synthesized, and prepared nanoparticles with zein and Puerarin. And the *Bletilla striata*polysaccharides with colonic mucosa repair effect was oxidized, and mixed with chitosan and β-sodium glycerophosphate to prepare thermosensitive hydrogel. Thermosensitive hydrogels were combined with nanoparticles to investigate their mucosal adhesion, retention, and permeability, as well as their therapeutic effects on ulcerative colitis. Thiolated-hyaluronic acid nanoparticles had good stability, and could be quickly converted into hydrogel at body temperature when combined with thermosensitive hydrogel. The nanoparticles-loaded thermosensitive hydrogel also was excellent at mucosal penetration, enhancing the retention time of drugs in colon, and effectively controlling drug release. *In vivo* ulcerative colitis treatment revealed that the nanoparticles-loaded hydrogel significantly repaired the colonic mucosa and inhibit colonic inflammation. Therefore, the thermosensitive hydrogel co-loaded nanoparticles will have a promising application in effective treatment of ulcerative colitis by topical administration.

Highlights

• Prepared a mucosal adhesive drug-loaded thiolated-hyaluronic acid nanoparticles.

• A novel *Bletilla striata* polysaccharides thermosensitivity hydrogel was developed.

• Nanoparticles-assembled thermosensitivity hydrogel as a new platform.

• Future perspectives of in-situ drug delivery of ulcerative colitis were discussed.

1. Introduction

Ulcerative colitis (UC) is a chronic inflammatory disease affecting the colon, which is characterized by recurrent and mucosal inflammation, and the incidence of UC is increasing globally. The pathogenesis of UC is multifactorial, involving genetic susceptibility, epithelial barrier defects, immune response disorders, and environmental factors[1]. As a chronic disease, there is no known treatment that can completely eradicate UC, other than colectomy, and patients are commonly treated with lifelong medication. Drugs can achieve disease remission and ensure a basic quality of life for patients[2]. It is most commonly in oral or topical administration (enema or suppository). Although oral preparation is convenient for administration and the compliance of the patients is quite good, it is difficult to avoid the first-pass effect of the liver on the drug. At the same time, the digestion and absorption of the drug in the stomach and small intestine, make it difficult to ensure that the concentration of the drug can be maintained after the drug reaches the colon. On the other hand, the common suppositories and enemas in local administration

can be administered in situ, which controls the concentration of the drug in the colon and avoids the loss of the drug, but there are also certain defects. For example, the suppository cannot reach above the junction of the sigmoid colon, and the enema is easy to leak and difficult to stay in the body, requiring many repeated administrations to make the drug work[3].

New colon-targeted drug delivery systems, such as nanoparticles, are frequently used for UC treatment by oral administration due to their excellent colon localization, ability to protect drugs, enhanced solubility of poorly water-soluble drugs, and control of drug release. As shortcomings in oral administration have exposed, researchers have begun modifying nanoparticles to enhance their stability in the stomach and small intestine[4], and to improve their adhesion at the target site[5], so that most of them can reach the target site to play a role. For example, hyaluronic acid (HA) has the function of targeting macrophages, and it enhances the adhesion of colon and the targeting of macrophages, after being modified into thiolated hyaluronic acid (HA-SH) to prepared into nanoparticles[6]. Furthermore, it can also be transformed into rectal administration by changing the mode of administration to improve the retention of drugs in the colorectal[7]. Rectal administration can make the nanoparticles reach the upper colon and more or less prolong the residence time. However, like other materials, nanoparticles are typically rapidly depleted to the outside due to the presence of feces, natural defecation, and defecation reflexes[8].

Polymer thermosensitive hydrogels are flowable and injectable fluid sols at room temperature, and they can automatically convert into hydrogels at body temperature and have strong adhesion properties. They have been used as carriers in the treatment of different diseases in recent years. For example, as an antibacterial wound dressing[9], as a myocardial cell carrier[10], or for promoting corneal epithelial regeneration[11]. Furthermore, there are also emerging studies on thermosensitive hydrogels as in situ drug delivery carriers for colon or rectum. Wang et al.[12] used an improved poloxamer thermosensitive hydrogel to carry growth factors and repair the mucosal barrier of the inflamed colon. Xue et al.[13] used thermosensitive hydrogel to enhance the adhesion time and therapeutic effect of Kangfuxin solution (KFX) in situ administration of colon. Chitosan (CS) drug-loading thermosensitive hydrogel has been proved to be safe and effective for in situ colon administration[14]. As a natural polymer, *Bletilla striata* polysaccharide (BSP) is frequently chosen as the preparation material of hydrogel, which has excellent mucosal repair effect[15]. At the same time, BSP has been shown to be effective in the treatment of colitis by modulating the intestinal flora, repairing damaged colon mucosa, and modulating inflammatory factors[16]. However, the solubility of the drug in the hydrogel and whether the hydrogel can control the stable release of the drug are also issues that need to be considered.

Therefore, the combination of the nano-drug carriers which can achieve drug targeting and sustained release and the polymer thermosensitive hydrogel carriers which can be used for local injection in situ therapy, is used for in situ administration of UC. As drug carriers, they can efficiently and accurately deliver drugs, that is, to improve efficacy and reduce systemic adverse reactions. The colorectal drug delivery platform of nanoparticles in combination with thermosensitive hydrogels has been used in the treatment of UC[3] and rectal cancer[17]. They avoid the rapid excretion of the nanoparticles, the insoluble

of the drug and the harm caused by or rapid release accumulation of the drug in the hydrogel, thereby improving the bioavailability of the drug.

Consequently, in this study, we modified HA to thiolated-hyaluronic acid (HA-SH) to prepare HA-SH-zein nanoparticles, which improved their mucosal permeability and adhesion in the colon. Puerarin (Pur), a Chinese herbal monomer that has therapeutic effects on UC by promoting goblet cell differentiation and repairing the submucosa of the colon[18], as a model drug was loaded in the HA-SH-zein NPs. BSP was chosen to prepare hydrogel, which was easier to form hydrogel with CS after oxidation. Then crosslinking agent β-GP was added to make it thermosensitive. The nanoparticles used the HA-SH as the shell, and the hydrogel was made from two kinds of natural polysaccharides. With the combination of NPs and hydrogel, the polysaccharides were cross-linked by hydrogen bond and Schiff base reaction, which could greatly shorten the gelation time and realize the adhesion and penetration of hydrogel in the colon. Summarily, we developed a novel platform (Pur@HA-SH-zein NPs in Hydrogel) for the treatment of UC through the combination of nanoparticles and thermosensitive hydrogels. And the *in vitro* release of Pur@HA-SH-zein NPs in Hydrogel and the therapeutic effect on DSS-induced acute UC model in mice were evaluated.

2. Materials and Method

2.1 Materials

Bletilla striata was provided by Sichuan Chinese Medicine Yinpian Co., Ltd. (Sichuan, China). Hyaluronic acid (Mw: 20 ~ 40w), chitosan (Mw = 20w, Dac degree: 85%), 3,3’-dithiobis(propionohydrazide), 2-(N-Morpholino) ethanesulfonic acid (MES), 4-(4,6-Dimethoxy-1,3,5-triazin-2-yl)-4-methylmorpholin-4-ium chloride (DMTMM), tris(2-carboxyethyl) phosphine hydrochloride (TCEP-HCl) were purchased from Shanghai Macklin Biochemical Co., Ltd. (Shanghai, China). Zein was purchased from Tokyo Chemical Industry Co., Ltd. (Tokyo, Japan). Puerarin (purity: 99%) was purchased from Chengdu Lemeitian Pharmaceutical Technology Co., Ltd. (Chengdu, China). β-sodium glycerophosphate (β-GP) and Coumarin-6 (C6) were purchased from Shanghai Aladdin Biochemical Technology Co., Ltd. (Shanghai, China). Dextran sodium sulfate (DSS, 40 kDa) was obtained from Seebio Biotech Co., Ltd. (Shanghai, China). IR-780 iodide was obtained from Sigma-Aldrich Co. (Steinheim, Germany).

2.2 Synthesis and Characterization of HA-SH

2.2.1 Synthesis of HA-SH

3,3'-Dithiobis (propanoic dihydrazide) solution (24.0 mg in 1.0 ml DMSO) and DMTMM solution (111.0 mg in 1.0 ml deionized water) were added dropwise to HA C1Xsolution (400.0 mg, in 50 ml 10.0 mM MES buffer (pH = 5.5)). The mixing solution was stirred at room temperature for 12h. Then, TCEP-HCl solution (143.0 mg in 5.0 ml deionized water) was added dropwise to the above solution and stirred for 3 h to obtain the resulting solution[19]. After dialysis, the solution was freeze-dried (Scientz-10ND, Scientz, China) and stored for later use.

2.2.2 The characterization of HA-SH

The infrared spectra of HA and HA-SH were detected by Fourier transform infrared spectrometer (FT-IR) (Spectrum One, America). In short, the sample was mixed with KBr, further pressed into thin slices, and scanned in the range of 400–4000 cm^{-1}. The ^{1}H NMR spectra of HA and HA-SH were obtained by Bruker AV600 nuclear magnetic resonance instrument (Bruker, Swit.) with heavy water as solvent.

2.3 Preparation and characterization of Pur@HA-zein NPs and Pur@HA-SH-zein NPs

2.3.1 Solubility of Zein

Zein (20 mg) was accurately weighed and dissolved in different solvents (2 ml, deionized water, anhydrous ethanol, and different concentrations of ethanol aqueous solution), separately. The solubility of zein in different solvents was observed after stirring at 360 rpm for 10 min.

2.3.2 Preparation of Pur@HA-zein NPs and Pur@HA-SH-zein NPs

Pur-loaded nanoparticles were prepared according to the previous reports[20]. In brief, precisely weighed Pur (4 mg) and zein (20 mg) completely dissolved in ethanol solution (2 ml, 80%, v/v). It was added dropwise to deionized water (6 ml) while stirring at 500 rpm for 20 min. After removing the residual ethanol by rotary evaporation (-0.1 MPa, 40℃). The above solution was added dropwise into the solution (6 ml) dissolved HA-SH or HA (1 mg) with stirring at 500 rpm for 20 min. The Pur@HA-zein NPs and Pur@HA-SH-zein NPs could be obtained after passing through the microfiltration membrane (0.8 μm).

2.3.3 Characterization of Pur@HA-zein NPs and Pur@HA-SH-zein NPs

The particle size distribution and ζ-potential of nanoparticles were measured by a dynamic light scattering instrument (LITESIZER500, Anton Paar, Austria). The morphology of Pur@HA-SH-zein NPs and Pur@HA-zein NPs was observed by transmission electron microscopy (TEM, JEM 1200X, JEOL, Japan). The physical loading of Pur in HA-zein NPs and HA-SH-zein NPs was characterized by Fourier transform infrared spectroscopy (FT-IR, Spectrum One, America).

The stability of the nanoparticles was determined. The particle size and zeta potential of Pur@HA-SH-zein NPs and Pur@HA-zein NPs were measured according to the agreed time for 7 days to characterize the stability of the two nanoparticles.

The encapsulation efficiency (EE) and drug loading efficiency (DL) of Pur@HA-SH-zein NPs and Pur@HA-zein NPs were determined by high performance liquid chromatography (HPLC, Thermo Ultimate 3000, America). Briefly, each of the two nanoparticle suspensions (1 ml) was accurately transferred into the centrifuge tube and centrifuged in a high-speed refrigerated centrifuge at 1.5×10^{4} rpm for 30 min after

sealing. 200 µl of the lower precipitate and the supernatant were taken, respectively, and diluted to 2 ml with ethanol (30%, v/v), and extracted by ultrasound for 1 h, respectively. After filtration by the 0.22 µm microfiltration membrane, of the filtrate (10 µl) was injected into HPLC and content of Pur was determined by a C_{18} chromatographic column (250 mm×4.6 mm, 5 µm, Thermo) at the maximum absorption wavelength of 250 nm, mobile phase of methanol-water (30: 70, v/v), flow rate of 1.0 ml min^{-1}. The EE and DL were calculated using the following Equation. 1–2:

EE=Amount of Pur loaded/Amount of Pur added × 100% (1)

DL=Amount of Pur loaded/total amount of NPs harvested ×100% (2)

2.4 Preparation of NPs-loaded OBSP/CS thermosensitive hydrogels

2.4.1 Preparation and characterization of BSP

Bletilla striata polysaccharides (BSP) was prepared according to the previous methods in the laboratory [21]. After 30 min of soaking in 95% ethanol, Bletilla striata powder was refluxed and extracted twice for 2 hours each time, and the filter residue was dried after filtration. The filter residue was refluxed and extracted twice with petroleum ether (60 ~ 90 ℃) for 2 hours each time, and filtered and dried. The filter residue was extracted twice with 40 times pure water and extract was concentrated. After the concentrated solution was deproteinized by Sevage method, the residual organic reagent was evaporated and 95% ethanol was added to obtain polysaccharides precipitation at 4 ℃ overnight. The precipitate of polysaccharides was collected and washed with different organic reagents. The crude BSP was purified by DEAE cellulose column (4×40 cm).

The polysaccharide content of the purified BSP was determined by the sulfuric acid-phenol method. The relative molecular weight of polysaccharide was determined by high performance gel permeation chromatography (HPGPC). The monosaccharide composition of BSP was determined by high performance liquid chromatography (HPLC).

2.4.2 Synthesis and characterization of OBSP

Oxidized BSP was synthesized by a modified method[22]. Briefly, BSP solution (3 g in 50 ml deionized water) and $NaIO_4$ solution (0.72 g in 50 ml deionized water) were mixed and reacted in the dark for 8 h, and then ethylene glycol (2 ml) was added to continue the shading reaction for 2 h. It was put into a dialysis bag (Mw ~ 3500), and dialyzed with distilled water at room temperature and vacuum for 3 d lyophilized to obtain OBSP of 20% oxidation degree[23]. Subsequently, the oxidation degree of BSP was determined through the hydroxylamine hydrochloride potentiometric titration[24, 25]. In short, OBSP (100 mg) was dissolved in hydroxylamine hydrochloride solution (25 ml, 0.25 M). The methyl orange as indicator, the HCl consumption by the reaction was titrated with standardized NaOH solution (0.1 M). All experiments were done at least in triplicate.

The infrared spectra of BSP and OBSP were detected by Fourier transform infrared spectrometer (FT-IR) (Spectrum One, America). In short, the sample was mixed with KBr, further pressed into thin slices, and scanned in the range of 400–4000 cm^{-1}. The ^{1}H NMR spectra of BSP and OBSP were obtained by Bruker AV600 nuclear magnetic resonance instrument (Bruker, Swit.) with heavy water as solvent.

2.4.3 Preparation of OBSP/CS Thermosensitive Hydrogel

According to the fact that CS and β-GP can form thermosensitive hydrogel[10, 26], OBSP/CS thermosensitive hydrogel was prepared. In short, CS was dissolved in acetic acid solution (1%, v/v) and configured into a CS solution (1%, m/v). Precisely weighed a certain mass of OBSP were dissolved in the above CS solution (2 ml) to obtain OBSP solutions of different concentrations (0, 0.5%, 1%, 1.5%, and 2%, m/v). At 4°C, β-GP solution (200 μl, 50%, m/v) was added into the mixed solution of OBSP/CS. After stirring for 3 min, the mixed solutions were placed in the 37°C water bath to observe the state of the mixed solution at different temperatures.

2.4.4 Preparation of NPs-loaded OBSP/CS Thermosensitive Hydrogels

Acetic acid was added to the prepared HA-SH-zein NPs suspension to make the concentration of acetic acid reach 1% (v/v). An appropriate amount of CS and OBSP were dissolved in the suspension respectively to make the concentration of CS in the mixed solution be 1% (m/v) and the concentration of OBSP be 0.5% and 1% (m/v). At 4°C, β-GP solution (50%, m/v) was added, stirred for 3 min, and placed in a water bath at 37°C to observe the state of the mixed solution at different temperatures.

2.5 Characterization of NPs-loaded OBSP/CS thermosensitive hydrogels

2.5.1 Gelation Times

The gelation times of four thermosensitive hydrogels (blank hydrogel $OBSP_{0.5}/CS_1$, $OBSP_1/CS_1$ and NPs-loaded hydrogel $OBSP_{0.5}/CS_1$-NPs, $OBSP_1/CS_1$-NPs) were determined by the vial inversion method. The polymer solution and β-GP solution were mixed and stirred at 4°C for 3 min, and placed in a 37°C water bath. The gelation time was measured by gently inverting the vial and observing that the mixture was no longer flowing. Each group was repeated 5 times.

2.5.2 Scanning Electron Microscope (SEM)

The cross-sections of four hydrogel samples after lyophilization were observed using a scanning electron microscope (SEM, Axio Imagerm2 EVO10, Germany). The hydrogel samples were freeze-dried after liquid nitrogen freezing and observed by coating with sputtered gold in vacuum.

2.5.3 Swelling Rate of the Hydrogel

The above four hydrogel samples after freeze-drying were weighed and placed in 20 ml simulated colonic fluid (SCF, pH = 7.4). The samples were taken out at the appointed time, and the water on the surface of the hydrogel was absorbed with filter paper. The swelling rate of the hydrogel was calculated using the following Equation. 3:

Swelling rate=$(W_t-W_0)/W_0\times100\%$ (3)

where the W_0 and W_t are the mass of hydrogel before and after swelling, respectively. Each assay was repeated three times.

2.5.4 Rheological Measurements

The rheological properties were determined by a rheometer (Anton Paar MCR302, Austria). The changes of storage modulus (G') and loss modulus (G") with temperature (20℃~ 40℃) were measured at a fixed frequency of 0.5 Hz, a fixed strain of 1%, and a heating rate of 1.0 ℃ min^{-1}.

2.6 Biocompatibility of Hydrogels *in Vitro*

The *in vitro* biocompatibility of the four hydrogels ($OBSP_{0.5}/CS_1$, $OBSP_1/CS_1$, $OBSP_{0.5}/CS_1$-NPs and $OBSP_1/CS_1$-NPs) in L929 cells was performed by the CCK-8 assay[27]. Different concentrations of hydrogel samples were immersed in DMEM medium supplemented with 10% fetal bovine serum at 37°C for 24 h to obtain different concentration extracts (0.625, 1.25, 2.5, and 5 mg ml^{-1}). L929 cells (5×10^4 cells per well) were inoculated in 96-well plates for 24 h, and the original culture medium was taken out and replaced with four hydrogel extracts of different concentrations (100 µl). Meanwhile, untreated cells were used as negative control and separate culture medium as background. The cells were cultured on 96-well plates and were incubated at 37℃ under an atmosphere of 5% CO_2. After incubation for 24 h, CCK-8 in serum-free medium (10µl) was added to each well and incubated for 2 h. The optical density (OD) at 450 nm was measured on a microplate reader to calculate the cell viability as reported before. Then the proliferation of L929 cells in 4 different concentrations of Pur@HA-SH-zein NPs in Hydrogel extract for 24 h, 48 h and 72 h were detected by live and dead cell staining.

2.7 Degradation of Hydrogels *in Vivo*

In vivo biocompatibility of thermosensitive hydrogels was investigated by subcutaneous injection[3]. Pur@HA-SH-zein NPs in Hydrogel (300 µl) was injected into the subcutaneous tissue of male ICR mice. The size of the hydrogels on the body surface of the mice was observed at the designated time points. After the mice were sacrificed, the skin tissue at the injection site was surgically removed to observe the state and size of the hydrogel in the mice.

2.8 *In Vitro* Release of Pur from NPs and Hydrogel

$OBSP_1/CS_1$-NPs were selected as drug carriers, and Pur was encapsulated into NPs to prepare hydrogels named Pur@HA-SH-zein NPs in Hydrogel. The *in vitro* release behavior of free Pur, Pur@HA-zein NPs, Pur@HA-SH-zein NPs and Pur@HA-SH-zein NPs in Hydrogel was determined by dialysis method using

simulated colon fluid (SCF) as the release medium[28, 29]. The samples were placed in the release medium SCF containing Tween-80 (0.5%) to promote Pur dissolution after being packed in a dialysis bag (Mw ~ 3500). The samples were shaken at 37°C and 80 rpm, and release medium (2 ml) was taken at the agreed time, and fresh SCF (2 ml) was supplemented. Above liquid (200 µl) was diluted to 2 ml with ethanol (30%, v/v) and ultrasonically extracted for 1 h. The extract was filtered through a 0.22 µm microfiltration membrane, and the content of Pur in the filtrate was determined by HPLC as mentioned above, and the cumulative release rate was calculated.

2.9 Adhesion of Hydrogels *in Vitro*

The adhesion of the hydrogel on the colon was investigated with pig colon *in vitro*[30]. Methylene blue (MB) instead of Pur was loaded into the NPs, and the NPs suspension was used to prepare the thermosensitive hydrogel MB@HA-SH-zein NPs in Hydrogel. The fresh pig colon tissue was rinsed with PBS (pH = 7.4) 3 times. A 10cm segment of the colon was cut longitudinally, and the mixture solution (500 µl) was evenly coated on the upper part of the colon and hung vertically to monitor the changes in the adhesion of the hydrogel with time under gravity. After that, the colons adhered to the hydrogel were immersed in SCF at 37°C for 2 h, and the adhesion of the hydrogel on the colon was observed.

2.10 Animal experiment

2.10.1 Animals and DSS Model Establishment

Male ICR mice (22 ~ 25 g) were provided by SPF Biotechnology Co., Ltd. (Beijing, China). The mice were placed in standard conditions and provided with food and distilled water at will in specific pathogen-free facilities. All animal studies were carried out according to the scheme approved by the animal welfare committee of Chengdu University of Traditional Chinese Medicine (SYXK (Chuan) 2020 – 214). The animals were allowed to acclimate for 1 week before the experiment. According to previous studies, ulcerative colitis in ICR mice was induced by drinking water containing 2.5% DSS.

2.10.2 Retention and Adhesion Effect of Different Preparations in Colon

IR780 iodide was used as a fluorescent probe instead of Pur. UC mice (3 mice per group) were given free IR780, IR780@HA-zein NPs, IR780@HA-SH-zein NPs and IR780@HA-SH-zein NPs in Hydrogel (IR780 0.5 mg kg^{-1}) by rectal administration, respectively. At the predetermined time points (0, 3, 6, 12, and 24 h) after rectal administration, anesthetizing mice with isoflurane, the changes of fluorescence intensity in mice were observed by in vivo imaging system IVIS (PerkinElmer). The mice were euthanized and colons were removed at 24 h to evaluate the distribution of the formulation in the colon.

2.10.3 Permeability of Different Preparations in Colonic Epithelium

To further investigate the targeted permeability of HA-SH-zein NPs in Hydrogel to macrophages *in vivo*, the fluorescent probe C6 was used instead of Pur. Intrarectal administration of free C6, C6@HA-zein NPs, C6@HA-SH-zein NPs or C6@ HA-SH-zein NPs in Hydrogel (C6 0.5 mg kg^{-1}) to UC mice, respectively. After 24 h of enema, the mice were sacrificed and the colon tissue was removed, washed thoroughly with PBS, and embedded in the optimal cutting temperature (OTC). The colon tissue was sectioned using a freezing microtome (Leica CM1950, Germany) and the colon sections (10 μm) were stained with Alexa Fluor 647 phallodine (AF647) and DAPI. The images were obtained by a fluorescence microscope (Leica DM6 B, Germany).

2.10.4 Therapeutic Effects of Different Preparations on DSS-induced UC in Mice

Male ICR mice were randomly divided into 6 groups (10 mice in each group): normal group, UC model group, Pur group, Pur@HA-zein NPs group, Pur@HA-SH-zein NPs group and Pur@HA-SH-zein NPs in Hydrogel group. The control group received no modeling and treatment, and the remaining groups were allowed to freely drink drinking water containing 2.5% DSS for 10 days. On the third day, the mice in each administration group were injected with 0.1 ml of different preparations (Pur 1.6 mg kg^{-1}) to the proximal colon by rectal administration, using a hose with a diameter of 1 mm connected with a syringe. After administration, the mice were kept upside down for 30 s, once every other day for 7 days. During the whole experiment, the body weight and disease activity index (DAI: weight loss (0–4), fecal bleeding (0 – 4), fecal consistency (0 – 4)) of mice were recorded daily. The scoring rules[3] are detailed in Table S1. On the final day, the mice were sacrificed and dissected, the colon was taken and the length was measured, and the spleen was weighed.

The colon segments of mice at 5 cm from the anus were collected, fixed with 4% paraformaldehyde, embedded in paraffin, and cut into 5 μm sections for hematoxylin-eosin (H&E) and periodic acid-Schiff (PAS) staining, respectively. Then the tissue morphology was observed under optical microscope.

Fresh colon tissues were collected to detect inflammatory cytokines. After the fresh colon was thoroughly homogenized, the colon supernatant was separated by centrifugation (10000rpm, 10min) and stored at -80℃. The concentrations of inflammatory cytokines TNF-α, IL-1β, IL-6 and IL-10 in colon tissue were detected according to the method on the ELISA kit (Multi Science, China).

2.11 Statistical Analysis

Data are expressed as mean ± standard deviation of at least three observations. Analysis of variance (ANOVA) and t-test were used for statistical comparison. Using statistical software GraphPad Prism 9 for statistical analysis, when $p < 0.05$, it is considered to be statistically significant.

3. Results and discussion

3.1 Synthesis of HA-SH

Figure 1A displayed the synthesis of HA-SH. Firstly, HA condensed with 3,3'-dithiobis (propionohydrazide) in MES acid buffer solution catalyzed by DMTMM. Then TCEP-HCl was added to reduce the disulfide bond and prepared. The ^{1}H NMR spectra of HA and HA-SH were shown in Fig. 1B. The peak at 3.0-3.9 ppm was the chemical shift of hydrogen produced on the sugar ring, and the peak near 1.99 ppm was the peak of the methyl group in HA. Compared with the ^{1}H NMR spectrum of HA, HA-SH showed two new low-intensity peaks at 2.68 ppm and 2.83 ppm, corresponding to two methylene groups on the substituent group, which proved that the sulfhydryl group was attached to HA. Comparing the FT-IR spectra of the two (Fig. 1C), HA has obvious asymmetric and symmetrical stretching vibration peaks belonging to carboxylates at 1610cm^{-1} and 1414cm^{-1}. The bending vibration of HA-SH near 1560cm^{-1} belongs to the amide II band N-H, indicating that HA formed a new amide bond in the synthesis reaction. And HA-SH increased the bending vibration peak belonging to -SH at 2528.22 cm^{-1}, which was consistent with the analysis results of ^{1}H NMR.

3.2 Characterization of Pur@HA-zein NPs and Pur@HA-SH-zein NPs

Preparation two kinds of Pur-loaded core-shell NPs by ethanol injection. We first chose the solvent of zein, according to the characteristics of zein dissolved in hydrous alcohol[31], solubility of zein in alcohol solutions (2 ml) of different concentrations (0, 20%, 40%, 60%, 80%, and 100%, v/v) was shown in Fig. 2G. Zein in anhydrous ethanol, pure water, and ethanol solution of 20% and 40% could not be dissolved totally, completely dissolved inethanol solution of 60% and 80%, but the clarity of 60% ethanol solution of zein was inferior than 80%. Thus 80% ethanol was selected as the solvent of zein to prepare NPs. The two NPs obtained were shown in Fig. 2A and D. The particle size of Pur@HA-zein NPs was 203.48 ± 7.86 nm, and the particle size of Pur@HA-SH-zein NPs was 164.58 ± 1.75 nm. At the same time, comparing the TEM of the two NPs (Fig. 2B and E), it could be seen that the two NPs were both core-shell structures, but the shell of Pur@HA-SH-zein NPs was more uniform and denser, and the shapes of these NPs were closer to spherical. The Pur@HA-zein NPs are not as well shaped as the former, with looser shells and uneven thicknesses. It sufficiently demonstrates the potential of HA-SH to prepare nanoparticles with smaller particle sizes and better structure. Comparing the above two kinds of NPs with core-shell structures and Pur@zein NPs, the suspensions of the three NPs were different in color and their ζ-potentials (Supporting Information Figure S1). All three NPs were negative potentials, but the potential of Pur@zein NPs was − 18.8 ± 3.2 mV. The potential of Pur@HA-zein NPs increased slightly to − 29.2 ± 1.8 mV, and Pur@HA-SH-zein NPs had the highest negative potential of − 32.0 ± 0.6 mV.

According to the FT-IR spectra of the two NPs (Fig. 2C and F), Pur had an aromatic conjugated carbonyl absorption band at 1633 cm^{-1}, and an aromatic nucleus absorption band at 1515 cm^{-1} and 1448 cm^{-1}[32]. In addition, there was a peak of 891 cm^{-1} in the fingerprint of Pur, which belonged to the substitution region of benzene ring[33]. In the FT-IR spectrum of zein, the vibrational peaks of -OH and -NH2 in zein appeared at 3320 cm^{-1}, at 1657 cm^{-1} due to stretching vibration of C = O, and at 1531 cm^{-1} due to bending vibration of-N-H[29]. After Pur was loaded into HA-zein NPs and HA-SH-zein NPs, its

characteristic peaks were significantly changed and were completely covered, indicating that Pur was successfully encapsulated into NPs.

The stability of the two core-shell NPs (Fig. 2H) was investigated. For 7 consecutive days, the particle size and ζ-potential of Pur@HA-zein NPs fluctuated considerably, and Pur@HA-SH-zein NPs remained relatively stable, which proved that HA-SH maintained the regular shape of NPs while maintaining the stability of the physical properties of NPs. The EE and DL of the two NPs were also different. The EE of Pur@HA-zein NPs was about 95.4%, and the DL was 16.11%. The EE of Pur@HA-SH-zein NPs increased to 97.26% and the DL also increased to 16.31%. The increase in EE and DL could be related to the difference in the morphological structure of the two NPs.

3.3 Basic properties of BSP

In this experiment, BSP that was isolated from the same batch as that used in our lab was used[34]. The total carbohydrate content of BSP determined by phenol-sulfuric acid method was 78.37%. The Mw and Mn of BSP were 2.36×10^5 g mol^{-1} and 6.63×10^4 g mol^{-1} according to HPGPC analysis. Monosaccharide analysis showed that BSP had two monosaccharides, mannose, and glucose, with the molar ratio of 3.13:1.

3.4 Synthesis and characterization of OBSP

OBSP was oxidized with $NaIO_4$ as shown in Fig. 3A. $NaIO_4$ was a highly specific selective oxidant and the oxidation degree of OBSP can be controlled by the ratio of $NaIO_4$ to BSP. The oxidation degree of OBSP was determined to be 19.17 ± 0.47% by the hydroxylamine hydrochloride method (Supporting Information Figure S2). The oxidized products OBSP and BSP were compared and analyzed using ^{1}H NMR and FT-IR. In the ^{1}H NMR spectrum (Fig. 3B), the sample showed a chemical signal belonging to the polysaccharide in the range of 3.0-3.9 ppm, and the chemical signals belonging to methyl in polysaccharides appeared at 2.1 ppm. The difference was that a new low-intensity peak belonging to the aldehyde group appeared near 9.1 ppm, which proved that some hydroxyl groups in BSP were oxidized to aldehyde groups. FT-IR spectra (Fig. 3C) showed that both BSP and OBSP had characteristic absorption peaks of polysaccharides at wavenumbers of 4000 – 400 cm^{-1}. The long and broad absorption peak at 3399 cm^{-1} was the O-H stretching vibrational peak of polysaccharides, and the faint absorption peak at 2925 cm^{-1} was the C-H stretching vibrational peak. Peaks at 1150 cm^{-1} and 1032 cm^{-1} indicated the presence of pyranose. In addition, the peaks at 877 cm^{-1} and 809 cm^{-1} also show mannose absorption[35]. Compared with unmodified BSP, OBSP showed an enhanced carbonyl (C = O) stretching vibration absorption peak at 1733 cm^{-1}, which indicated that some hydroxyl groups on the molecule of BSP were changed into aldehyde groups after oxidation, which was consistent with the conclusion of ^{1}H NMR.

3.5 Characterization of blank OBSP/CS thermosensitive hydrogel

According to previous studies, BSP could react with CS to form a hydrogel after oxidation to form aldehyde groups. However, the required degree of oxidation of BSP was generally higher, the concentration of CS was also higher, and the reaction between the two required heating to a higher temperature. CS could form a kind of thermosensitive hydrogel with β-GP, which realized the transition from flow state to solid state when the temperature is about 37 ℃. We combined the two preparation methods of hydrogel to prepare OBSP/CS thermosensitive hydrogel. Firstly, the concentration of OBSP and CS was selected (Supporting Information Figure S3). When the concentration of CS was fixed at 1% (m/v), the concentration of OBSP increased sequentially. When the concentration of OBSP is 1.5% (m/v) and 2% (m/v), the hydrogel has been formed at 4℃, which was not thermosensitive. Without OBSP, due to the decrease of the concentration of CS, it took a long time to transform from solution to hydrogel after adding β-GP, almost impossible to form hydrogel. Only when the concentrations of OBSP were 0.5% (m/v) and 1% (m/v) could the mixture transit from solution to gel with increasing temperature.

The interaction between the molecules of the hydrogels was analyzed by FT-IR spectrogram of OBSP/CS hydrogels (Fig. 3D). In the CS spectrum, the broad peak at 3437 m^{-1} was attributed to the stretching vibrations of O-H and N-H. The characteristic absorption peak of amino group was covered by the absorption peak of O-H. The two peaks at 2924 cm^{-1} and 2874 cm^{-1} belonged to the stretching vibration of C-H. The stretching vibration of C = O at 1661 cm^{-1} and the bending vibration of primary amine group at 1598 cm^{-1} overlapped with that of amide II, which proved the existence of amino group in CS[36]. There was an asymmetric stretching vibration peak of -PO_4^{3-} in β-GP at 1080 cm^{-1} and a symmetrical stretching vibration peak at 976 cm^{-1}[10]. The symmetrical vibration peak of C = O belonging to OBSP at 1730 cm^{-1} in the hydrogel was significantly weakened, and the absorption peak belonging to C = N appeared at 1644 cm^{-1}, which proved that OBSP and CS were chemically crosslinked, that is, Schiff bonds were generated[24]. Due to the formation of hydrogen bonds between the O-H on the CS and the -PO_4^{3-} on the β-GP, the C = O stretching vibration peak also moved to the lower wave number, which strengthened the peak width and intensity of 1644 cm^{-1}. The absorption bands of O-H and N-H were also moving to the low wavenumber direction (3401 cm^{-1}), and the peak width was blunt, which also meant that some hydrogen bonds were formed.

3.6 Characterization of NPs-loaded OBSP/CS thermosensitive hydrogel

According to the formation of blank OBSP/CS thermosensitive hydrogels, 1% (m/v) CS was selected to mix 0.5% and 1% (m/v) OBSP to prepare hydrogels loaded with HA-SH-zein NPs, respectively. The above four hydrogels were named as $OBSP_{0.5}/CS_1$, $OBSP_1/CS_1$, $OBSP_{0.5}/CS_1$-NPs and $OBSP_1/CS_1$-NPs, respectively. The hydrogel formation time (Fig. 4A and B) was determined by the inverted bottle method. At 4°C, the four mixtures could flow. At 37°C, the mixtures could be formed at different times, and the gel time is 90.2 ± 4.58 s, 56.6 ± 3.61 s, 67.8 ± 2.79 s, and 46.0 ± 2.28 s, respectively. With the increase of OBSP concentration, it was easier to form hydrogen bonds or Schiff base reaction between OBSP, CS and β-GP,

thus shortening the gelation time. Due to the addition of core-shell NPs with HA-SH as a shell, hydrogen bonds may also be created between the blank hydrogel with NPs, which significantly shortens the gel formation time. However, the gelation time of $OBSP_1/CS_1$ was shorter than that of $OBSP_{0.5}/CS_1$-NPs, so it could be seen that the effect of concentration on gelation time was greater than that of loaded nanoparticles. Pur was replaced by Rhodamine to prove the rapid gelation of $OBSP_1/CS_1$-NPs. When the hydrogel solution was injected into 37℃ warm water with a syringe, the hydrogel solution is quickly converted into the hydrogel state and will not be dissolved in water (Supporting Information Video S1). The gelation process of four hydrogels was characterized by rheometer (Fig. 4E). With the increase of temperature, the storage modulus (G') of the hydrogel increased rapidly, and the transition temperature (G' = G") of the hydrogel decreased. $OBSP_{0.5}/CS_1$ changed from liquid to gel state at 29°C, and the remaining three hydrogels gradually gelled at 20°C (G' > G"). It was because the higher OBSP concentration made it easier to generate chemical crosslinking with CS and form intramolecular hydrogen bonds, which enhances the hydrophobic effect of the polymer, resulting in a decrease in gelation temperature. It could be seen that the concentration of OBSP had a great influence on the rheological behavior of the hydrogel, and the addition of NPs could also increase the G' of the hydrogel, which was consistent with the gelation time of the four hydrogels.

The microstructure of the natural cross-section of the four hydrogels after freeze-drying was observed by SEM (Fig. 4C). The cross section is distributed with many micropores, forming a continuous and uniformly distributed 3D network structure inside the hydrogel. Comparing the pores between the four hydrogels, the hydrogel with higher concentration of OBSP had more uniform and dense pores. The pore size of the hydrogel also became smaller after the addition of NPs. This may be that the addition of NPs increased the crosslinking degree of the hydrogel and reduced the pore size. In Fig. 4D, the swelling curves of four freeze-dried hydrogels in SCF were illustrated. The water absorption of the hydrogel in the initial stage (the first 1 h) showed a steep increase trend, and then the swelling rate began to increase with time, and gradually flattened out. The swelling rate of the four hydrogels remained essentially balanced at about 4 h. The swelling ratio of the two blank hydrogels eventually stabilized at about 300%. The swelling ratio of $OBSP_{0.5}/CS_1$ was slightly larger than that of $OBSP_1/CS_1$ due to its larger pore size and easier access to large amounts of free water. The swelling ratio of NPs-loaded hydrogel can reach about 500% (the swelling ratio of $OBSP_{0.5}/CS_1$-NPs was 567.6 ± 14.8%, and the swelling ratio of $OBSP_1/CS_1$-NPs was 487.4 ± 10.6%). This might be because the addition of NPs increased the porosity and made the hydrogel absorb more water. However, the four hydrogels had relatively small swelling rates, suggesting that they had some role in absorbing the exudate after it entered the colon, and did not over-absorb the fluid expansion and cause intestinal deformation.

3.7 Release of Pur *in vitro*

Based on the characterization of the hydrogel, we selected $OBSP_1/CS_1$-NPs as the drug carrier for NPs-loaded hydrogel, and encapsulated Pur in the NPs, named Pur@HA-SH-zein NPs in Hydrogel. The concentrations of Pur released from different preparations (Free Pur, Pur@HA-zein NPs, Pur@HA-SH-zein

NPs, and Pur@HA-SH-zein NPs in Hydrogel) in SCF over continuous time were compared to evaluate the drug release in the colon after they entered the colon in situ. The cumulative release of Pur was shown in Fig. 4F. Free Pur was rapidly released in SCF and totally released at 12 h with the cumulative release of 99.57%. When Pur was encapsulated in the two NPs, the release rate of Pur@HA-zein NPs in the first 10 h was close to that of the Free Pur and the cumulative release rate at 48 h was 94.8%, which may be related to the fact that HA in digestive juices was easy to be degraded uncontrollably and spread throughout the body, and these nanoparticles were not stable enough to prematurely expose drugs[37, 38]. However, the release rate of Pur@HA-SH-zein NPs was significantly reduced and stabilized at about 24 h, with a cumulative release of 91.00%. The rate of release of Pur@HA-SH-zein NPs in Hydrogel was significantly more stable and slower, with essentially complete release at 48h and a cumulative release rate of 77.61%. NPs were prone to burst release after entering the colon, which was not conducive to treatment. When the drug-loaded NPs were combined with the hydrogel, based on the swelling effect of the hydrogel, it could be slowly released in colon at a sustained rate, which was beneficial to its therapeutic effect in UC.

3.8 *In vitro* biocompatibility and *in vivo* degradation of hydrogel

The cytotoxicity of four hydrogels on L929 cells was detected using the CCK-8 method. Figure 5A shown that the cell survival rate decreases when the concentration of the hydrogel extract was increased. And the cell survival rate of the NPs-loaded hydrogel was slightly lower than blank hydrogel, probably due to the increased polymer type. However, even if the hydrogel $OBSP_1/CS_1$-NPs is highly concentrated (5 mg ml^{-1}), the cell survival rate was above 75%. The *in vitro* biocompatibility of Pur@HA-SH-zein NPs in Hydrogel was further investigated using live and dead cell staining. L929 cells were cultured in a medium containing different concentrations of hydrogel extract to quantify cell viability. After incubation for 24 h, 48 h and 72 h, the cells were observed by LSCM (Fig. 5B). The cells could survive on each concentration of hydrogel and proliferate in large quantities. The above results indicated that the hydrogel had extremely low cytotoxicity and could be used as a platform for drug delivery. Pur had no effect on cell proliferation and was certain security.

Subsequently, *in vivo* biodegradability and biocompatibility of Pur@HA-SH-zein NPs in Hydrogel were evaluated (Supporting Information Figure S4). The mixture solution (300 μl) was subcutaneously injected into the back of ICR mice. Hydrogel formation was clearly observed 10 min after injection, demonstrating that Pur@HA-SH-zein NPs in Hydrogel was excellently thermosensitive and able to form hydrogels quickly and efficiently. The size of the hydrogel on the surface of mice and the degradation *in vivo* were observed at the scheduled time. The hydrogel gradually became smaller in mice, and only a small amount of flaky hydrogel was dispersed at 28 days, indicating that it was biodegradable and could be degraded slowly *in vivo*. Hydrogel degradation is mainly due to surface erosion (degradation of the polymer network structure) and bulk erosion (fracture of chemical bonds in the polymer) [39].

3.9 *In vitro* adhesion and *in vivo* retention, distribution, and infiltration

Thermosensitive hydrogel was selected as the carrier of rectal administration for the treatment of UC. This was because the thermosensitive hydrogel was fluid in generally and able to transform into solidify to adhere on the colon in 37℃, so as to avoid the drug being excreted when administered due to the rejection of the animal. We replaced Pur with methylene blue (MB) to prepare MB-loaded NPs-hydrogels. Coating MB@HA-SH-zein NPs in Hydrogel evenly on the upper end of the vertically suspended inner wall of the pig colon in 37℃, the liquid mixture adhered on the inner wall of the colon and began to flow over time under the action of gravity (Fig. 5C). Immersing the colon segments attached with hydrogel in SCF at 37℃ for 2 h, the hydrogel remained attached to the mucosal surface in its previous form without dilution or detachment (Fig. 5D). Because CS and OBSP were able to generate hydrogen bonds with some molecules on the surface of the colonic mucosa to enhance adhesion. HA-SH has been shown to improve the intestinal retention effect of NPs by instantaneously forming disulfide bonds with mucin components[6].

In order to confirm that HA-SH-zein NPs in Hydrogel increased the retention of drugs in colon and were degraded under prolonged incubation, we prepared four preparations labeled with IR780 and administered them via rectal administration to UC mice. The images were collected by a living animal imager to evaluate the retention effect in the colon. The change of fluorescence intensity in mice reflected the retention of IR780 *in vivo*, and the fluorescence in colon reflects the distribution of IR780. After administration, as shown in Fig. 6A, the four preparations shown strong fluorescence at the administration site. However, it was obvious that IR780, IR780@HA-zein NPs and IR780@HA-SH-zein NPs all showed fluorescence in the anus of mice, which may be due to the defecation reflex of mice and the liquid that cannot adhere to the colon was discharged and remains in the anus. Due to the peristalsis of colon, the preparation began to distribute in the body at 3 h after administration, so the fluorescence was stronger than 0 h. The fluorescence of the additional three groups began to weaken after 6 h, and only weak fluorescence signal was observed at 12 h, while IR780@HA-SH-zein NPs in Hydrogel remained near the administration site. Strong fluorescence was still seen *in vivo* for IR780@HA-SH-zein NPs in Hydrogel at 24 h, but the fluorescence of free IR780 group was totally could not be observed. The fluorescence of IR780@HA-zein NPs and IR780@HA-SH-zein NPs appeared near the anus. Perhaps due to the peristalsis of colon, the NPs reached the end of the rectum, where there was no hair occlusion near the anus, showing the fluorescence. These results indicated that HA-SH-zein NPs in Hydrogel could prolong the retention time of drugs in the colon, which was beneficial for the long-term maintenance of effective drug concentrations in the colon for the treatment of UC. As shown in Fig. 6B, the distribution of IR780 in the colon was markedly reflected by detection of fluorescence in colon at 24 h. There was only weak fluorescence in the colon of the free IR780 group. Fluorescence in the colon of the IR780@HA-zein NPs and IR780@HA-SH-zein NPs groups appeared at the junction of the colon end and the anus, which was consistent with the *in vivo* results. IR780@HA-SH-zein NPs in Hydrogel shown strong fluorescence and

uniform distribution in the colon. It was revealed that the hydrogel was excellent colon-adhesion, nearly unaffected by defecation reflex, and can adhere to the colon for a long time.

To verify whether macrophages in colitis tissues could preferentially uptake HA-SH-zein NPs, C6 was used instead of Pur to prepare NPs, and frozen sections were immunostained with the F4/80 antibody labeled with AF 647. As shown in Fig. 6C, the green fluorescence of free C6 group in colon tissue was weak, indicating that it did not penetrate colon tissue well. The other three groups contained HA, and their green fluorescence was combined with the red fluorescence of F4/80, indicating the selectivity of HA to macrophages. However, this selectivity was also different depending on the intensity of green fluorescence. The green fluorescence signal of C6@HA-SH-zein NPs in Hydrogel was the strongest, which was distributed throughout the colon tissue and perfectly coincided with the red fluorescence signal of F4/80. It was proved that C6@HA-SH-zein NPs in Hydrogel can efficiently allow C6 to cross the mucosal barrier into colon tissue and has great selectivity for colon macrophages (F4/80).

3.10 *In vivo* therapeutic effect on DSS-induced UC in mice

To determine whether Pur@HA-SH-zein NPs in Hydrogel could improve the therapeutic effect of Pur on UC, we designed the experiment according to Fig. 7A. UC in ICR mice was induced by 2.5% DSS for 10 days, with treatment beginning on the third day. The relevant indicators of the normal control group and the UC model DSS group were compared to determine whether the model was successful. We also compared the therapeutic effects of free Pur, Pur@HA-zein NPs and Pur@HA-SH-zein NPs with the hydrogel group, in which the dose of Pur was 1.6 mg kg^{-1}. As shown in Fig. 7B, the color of the colons of the DSS group was significantly deeper than that of the control group, and it was obviously shortened and swollen. The four preparation treatment groups effectively alleviated colorectal shortening and color deepening to varying degrees, suggesting that Pur could improve UC to a certain extent. The therapeutic effect of free Pur was relatively poor. Pur@HA-SH-zein NPs was better than that of Pur@HA-zein NPs group, and the efficacy of Pur@HA-SH-zein NPs in Hydrogel was the best. It could be seen from the weight change curve, DAI score, and colon length of mice (Fig. 7C-E) that Pur@HA-SH-zein NPs in Hydrogel was significantly to improve UC caused by DSS, and the effect was better than other groups. As shown in Fig. 7F, the spleen index of the DSS group was higher than that of the normal group, indicating that inflammation could cause splenomegaly. The treatment group showed remission of splenomegaly and reduced spleen index, but only the Pur@HA-SH-zein NPs in Hydrogel showed significant differences compared to the DSS group. The remaining three treatment groups reduced the spleen index but the difference was not obvious. It suggested that the Pur@HA-SH-zein NPs in Hydrogel group had the best efficacy and was superior to the other three treatment groups.

The inflammation and therapeutic effect of the colon were observed by H&E and PAS staining (Fig. 8A). In the H&E staining tissue sections, the normal group of mice had normal colon pathology morphology, mucosal integrity, and no inflammatory cell infiltration. The tissue crypts of the DSS group were damaged, inflammatory cell infiltration was obvious, and the mucosa was eroded. All four treatment groups improved the destruction of this colitis tissue, and the recovery of UC tissue after treatment with

Pur@HA-SH NPs in Hydrogel was the best, which was because BSP could repair the damaged mucous membrane of inflamed colon. The result demonstrated that HA-SH NPs in Hydrogel was a reliable platform for UC treatment. PAS staining was mucin glycoprotein secreted by goblet cells[40]. Mucin was abundant in the control group, and the goblet cells were abundant and evenly distributed. The goblet cells in the DSS group were almost destroyed. Pur could promote the differentiation of goblet cells and the secretion of mucin[18], so all the treatment groups protected and repaired the goblet cells of the colon. The number of goblet cells in the Pur@HA-SH NPs in Hydrogel group was much more than that in the other three treatment groups, indicating that HA-SH NPs in Hydrogel could enhance the protection and differentiation of Pur on goblet cells and treat UC well. This was consistent with the results of H&E staining.

Inflammatory factors could also reflect the severity of UC. TNF-α, IL-1β and IL-6 are pro-inflammatory factors expressed by M1 macrophages, and IL-10 is an anti-inflammatory factor secreted by M2 macrophages[41]. Studies have shown that Pur can effectively reduce inflammatory factors in the treatment of UC[42], and BSP can regular the inflammatory factors such as reduction the levels of TNF-α and IL-1β, and up-regulation of IL-10[16]. By detecting the contents of inflammatory factors TNF-α, IL-1β, IL-6 and IL-10 in UC tissues (Fig. 8B-E), the levels of pro-inflammatory factors in the DSS group were significantly increased. Pur can effectively reduce the levels of TNF-α, IL-1β and IL-6. HA-SH NPs in Hydrogel could improve the ability of Pur to reduce these pro-inflammatory factors and improve colon inflammation. Pur@HA-SH NPs in Hydrogel also significantly increased the content of IL-10 to improve the anti-inflammatory ability of Pur. In summary, Pur@HA-SH NPs in Hydrogel can effectively treat UC and modulate the expression of inflammatory factors.

4. Conclusion

Ulcerative colitis is a complex inflammatory disease. The diffuse inflammation of the submucosa and the destruction of the goblet cells are its main characteristics. Therefore, alleviating inflammation and promoting the differentiation of goblet cells are the main aims of ulcerative colitis treatment. Treatment of ulcerative colitis with in-situ administration can greatly reduce drug loss, improve drug bioavailability, and extend residence time in the administration site to exert the retention effect of the drug. Therefore, a novel drug delivery platform (HA-SH-zein NPs in Hydrogel) was prepared in this study, in which drug-loaded nanoparticles combined with a thermosensitive hydrogel, to enable direct model drug (puerarin) perfusion at the site of colonic inflammation. The drug delivery platform prepared by thiolated-hyaluronic acid can improve the stability and drug loading of nanoparticles, and enhance the sustained release effect of the drugs. The thermosensitivity of oxidized *Bletilla striata* polysaccharides/chitosan hydrogel was realized by β-GP. The drug delivery platform achieve slow release of the drug and increase retention time in the colon for therapeutic effect. This novel drug delivery platform has superior biocompatibility, improves the macrophage penetration of puerarin, and shows to effectively treat DSS-induced ulcerative colitis in mice. While relieving submucosal inflammation, it can enhance the differentiation of goblet cells, regulate the expression of various inflammatory factors, and inhibit the development of inflammation. To sum up, we constructed a carrier of *Bletilla striata* polysaccharide thermosensitive

hydrogel containing thiolated-hyaluronic acid and zein nanoparticles to efficiently deliver drugs through rectal administration, thus providing a new idea and approach to in-situ drug delivery for the treatment of ulcerative colitis.

Abbreviations

AF 647, Alexa Fluor 647; **β-GP**, β-sodium glycerophosphate;

BSP, *Bletilla striata* polysaccharide; **C6**, coumarin-6;

CS, chitosan; **DAI**, disease activity index;

DAPI, 4',6-diamidino-2-phenylindole; **DL**, drug loading efficiency;

DMEM, dulbecco's modified eagle medium; **DMSO**, dimethylsulfoxide;

DMTMM, 4-(4,6-Dimethoxy-1,3,5-triazin-2-yl)-4-methylmorpholin-4-ium chloride;

DSS, dextran sodium sulfate; **EE**, encapsulation efficiency;

FT-IR; Fourier transform infrared; **H&E**, hematoxylin-eosin;

HA, hyaluronic acid; **HA-SH**, thiolated-hyaluronic acid;

HPLC, high performance liquid chromatography;

LSCM, laser scanning confocal microscopy; **MB**, methylene blue;

MES, 2-(N-Morpholino) ethanesulfonic acid; **NMR**, nuclear magnetic resonance;

NPs, nanoparticles; **OBSP**, oxidized *Bletilla striata* polysaccharide;

OD, optical density; **OTC**, optimal cutting temperature;

PAS, periodic acid-Schiff; **Pur**, puerarin;

SCF, simulated colonic fluid; **SEM**, scanning electron microscope;

TCEP-HCl, tris(2-carboxyethyl) phosphine hydrochloride;

TEM, ransmission electron microscopy; **UC**, ulcerative colitis.

Declarations

CRediT author statement

Shiyi Zhao: Conceptualization, Writing - original draft, Writing - review & editing. Junbo Zhang: Data curation, methodology, validation. Mengyu Qiu: Investigation, data curation, visualization. Yusen Hou: Investigation, project administration. Xuebo Li: Software, investigation, project administration. Guofeng Zhong: Investigation, project administration. Kaijun Gou: Data curation. Jingjing Li: Data curation. Chen Zhang: Writing - review & editing. Yan Qu: Writing - review & editing, Supervision. Xiao Wang: Writing - review & editing, Supervision.

Declaration of competing interest

The authors declare that they have no known competing financial interests or personal relationships that could have appeared to influence the work reported in this paper.

Data availability

Data will be made available on request.

Acknowledgments

The authors acknowledge Prof. Yan Qu and Dr. Chen Zhang for their fruitful discussions and suggestions during the preparation of this manuscript. This work is supported by the Natural Science Foundation of Sichuan Province (No. 2022NSFSC0373), the Natural Science Foundation of Sichuan Province (No.2023YFS0348), the China Postdoctoral Science Foundation (2021M690488), the Central Guidance on Local Science and Technology Development Fund of Sichucan (No. 2022ZYD0099).

Appendix A. Supplementary data

Supplementary Information on some experiments (file type, WORD).

References

1. Ungaro R, Mehandru S, Allen PB, Peyrin-Biroulet L, Colombel J-F: Ulcerative colitis. Lancet. 2017; 389:1756-1770.
2. Kayal M, Shah S: Ulcerative Colitis: Current and Emerging Treatment Strategies. Journal of Clinical Medicine. 2019; 9:94.
3. Guo Z, Bai Y, Zhang Z, Mei H, Li J, Pu Y, Zhao N, Gao W, Wu F, He B, Xie J: Thermosensitive polymer hydrogel as a physical shield on colonic mucosa for colitis treatment. Journal of Materials Chemistry B. 2021; 9:3874-3884.
4. Yuan H, Chen C, Chai G, Du Y, Hu F: Improved Transport and Absorption through Gastrointestinal Tract by PEGylated Solid Lipid Nanoparticles. Molecular Pharmaceutics. 2013; 10:1865-1873.
5. Liu H, Cai Z, Wang F, Hong L, Deng L, Zhong J, Wang Z, Cui W: Colon-Targeted Adhesive Hydrogel Microsphere for Regulation of Gut Immunity and Flora. Advanced Science. 2021; 8:e2101619.

6. Tian H, He Z, Sun C, Yang C, Zhao P, Liu L, Leong KW, Mao H-Q, Liu Z, Chen Y: Uniform Core-Shell Nanoparticles with Thiolated Hyaluronic Acid Coating to Enhance Oral Delivery of Insulin. Advanced Healthcare Materials. 2018; 7:e1800285.
7. Nunes R, Araújo F, Tavares J, Sarmento B, Neves Jd: Surface modification with polyethylene glycol enhances colorectal distribution and retention of nanoparticles. European Journal of Pharmaceutics and Biopharmaceutics. 2018; 130:200-206.
8. Melo M, Nunes R, Sarmento B, Neves Jd: Rectal administration of nanosystems: from drug delivery to diagnostics. Materials Today Chemistry. 2018; 10:128-141.
9. Fang X, Liu Y, Zhang M, Zhou S, Cui P, Hu H, Jiang P, Wang C, Qiu L, Wang J: Glucose oxidase loaded thermosensitive hydrogel as an antibacterial wound dressing. Journal of Drug Delivery Science and Technology. 2022; 76:103791.
10. Ke X, Li M, Wang X, Liang J, Wang X, Wu S, Long M, Hu C: An injectable chitosan/dextran/beta - glycerophosphate hydrogel as cell delivery carrier for therapy of myocardial infarction. Carbohydrate Polymers. 2020; 229:115516.
11. Tang Q, Luo C, Lu B, Fu Q, Yin H, Qin Z, Lyu D, Zhang L, Fang Z, Zhu Y, Yao K: Thermosensitive chitosan-based hydrogels releasing stromal cell derived factor-1 alpha recruit MSC for corneal epithelium regeneration. Acta Biomaterialia. 2017; 61:101-113.
12. Wang L, Xu J, Xue P, Liu J, Luo L, Zhuge D, Yao Q, Li X, Zhao Y, Xu H: Thermo-sensitive hydrogel with mussel-inspired adhesion enhanced the non-fibrotic repair effect of EGF on colonic mucosa barrier of TNBS-induced ulcerative colitis rats through macrophage polarizing. Chemical Engineering Journal. 2021; 416:129221.
13. Xue P, Wang L, Xu J, Liu J, Pan X, Zhao Y, Xu H: Temperature-sensitive hydrogel for rectal perfusion improved the therapeutic effect of Kangfuxin liquid on DSS-induced ulcerative colitis mice: The inflammation alleviation and the colonic mucosal barriers repair. International Journal of Pharmaceutics. 2020; 589:119846.
14. Xu J, Tam M, Samadei S, Lerouge S, Barralet J, Stevenson MM, Cerruti M: Mucoadhesive chitosan hydrogels as rectal drug delivery vessels to treat ulcerative colitis. Acta Biomaterialia. 2017; 48:247-257.
15. Gou K, Li Y, Qu Y, Li H, Zeng R: Advances and prospects of Bletilla striata polysaccharide as promising multifunctional biomedical materials. Materials & Design. 2022; 223:111198.
16. Wang C: Anti-ulcerative colitis function of Bletilla striata polysaccharide Master. Soochow University, 2018.
17. Din Fu, Choi JY, Kim DW, Mustapha O, Kim DS, Thapa RK, Ku SK, Youn YS, Oh KT, Yong CS, et al: Irinotecan-encapsulated double-reverse thermosensitive nanocarrier system for rectal administration. Drug Delivery. 2017; 24:502-510.
18. Wu Y, Li Y, Ruan Z, Li J, Zhang L, Lu H, Xu Z: Puerarin Rebuilding the Mucus Layer and Regulating Mucin-Utilizing Bacteria to Relieve Ulcerative Colitis. Journal of Agricultural and Food Chemistry. 2020; 68:11402-11411.

19. Cai Z, Huang K, Bao C, Wang X, Sun X, Xia H, Lin Q, Yang Y, Zhu L: Precise Construction of Cell-Instructive 3D Microenvironments by Photopatterning a Biodegradable Hydrogel. Chemistry of Materials. 2019; 31:4710-4719.
20. Chen S, Han Y, Huang J, Dai L, Du J, McClements DJ, Mao L, Liu J, Gao Y: Fabrication and Characterization of Layer-by-Layer Composite Nanoparticles Based on Zein and Hyaluronic Acid for Codelivery of Curcumin and Quercetagetin. ACS Applied Materials & Interfaces. 2019; 11:16922-16933.
21. Qu Y, Li C, Zhang C, Zeng R, Fu C: Optimization of infrared-assisted extraction of Bletilla striata polysaccharides based on response surface methodology and their antioxidant activities. Carbohydrate Polymers. 2016; 148:345-353.
22. Chen Z, Cheng L, He Y, Wei X: Extraction, characterization, utilization as wound dressing and drug delivery of Bletilla striata polysaccharide: A review. International Journal of Biological Macromolecules. 2018; 120:2076-2085.
23. Yang L, Han Z, Chen C, Li Z, Yu S, Qu Y, Zeng R: Novel probiotic-bound oxidized Bletilla striata polysaccharide-chitosan composite hydrogel. Materials Science and Engineering C: Materials for Biological Applications. 2020; 117:111265.
24. Chen C, Zhou P, Huang C, Zeng R, Yang L, Han Z, Qu Y, Zhang C: Photothermal-promoted multi-functional dual network polysaccharide hydrogel adhesive for infected and susceptible wound healing. Carbohydrate Polymers. 2021; 273:118557.
25. Zhao H, Heindel ND: Determination of degree of substitution of formyl groups in polyaldehyde dextran by the hydroxylamine hydrochloride method. Pharm Res. 1991; 8:400-402.
26. Hao T, Wen N, Cao JK, Wang HB, Lu SH, Liu T, Lin QX, Duan CM, Wang CY: The support of matrix accumulation and the promotion of sheep articular cartilage defects repair in vivo by chitosan hydrogels. Osteoarthritis Cartilage. 2010; 18:257-265.
27. Tang Q, Lu B, He J, Chen X, Fu Q, Han H, Luo C, Yin H, Qin Z, Lyu D, et al: Exosomes-loaded thermosensitive hydrogels for corneal epithelium and stroma regeneration. Biomaterials. 2022; 280:121320.
28. Wang X, Gu H, Zhang H, Xian J, Li J, Fu C, Zhang C, Zhang J: Oral Core-Shell Nanoparticles Embedded in Hydrogel Microspheres for the Efficient Site-Specific Delivery of Magnolol and Enhanced Antiulcerative Colitis Therapy. ACS Applied Materials & Interfaces. 2021; 13:33948-33961.
29. Zhang C, Wang X, Xiao M, Ma J, Qu Y, Zou L, Zhang J: Nano-in-micro alginate/chitosan hydrogel via electrospray technology for orally curcumin delivery to effectively alleviate ulcerative colitis. Materials & Design. 2022; 221:110894.
30. Zhao P, Xia X, Xu X, Leung KKC, Rai A, Deng Y, Yang B, Lai H, Peng X, Shi P, et al: Nanoparticle-assembled bioadhesive coacervate coating with prolonged gastrointestinal retention for inflammatory bowel disease therapy. Nature Communications. 2021; 12:7162.
31. Paliwal R, Palakurthi S: Zein in controlled drug delivery and tissue engineering. Journal of Controlled Release. 2014; 189:108-122.

32. Wang Y, Yang M, Qin J, Wa W: Interactions between puerarin/daidzein and micellar casein. Journal of Food Biochemistry. 2022; 46:e14048.
33. Li N: Study on puerarin targeting nanoparticle for vascular inflammation. Master. Jiangxi University of Chinese Medicine, 2021.
34. Zhou P, Zhao S, Huang C, Qu Y, Zhang C: Bletilla striata polysaccharide microneedle for effective transdermal administration of model protein antigen. Int J Biol Macromol. 2022; 205:511-519.
35. Liao Z, Zeng R, Hu L, Maffucci KG, Qu Y: Polysaccharides from tubers of Bletilla striata: Physicochemical characterization, formulation of buccoadhesive wafers and preliminary study on treating oral ulcer. International Journal of Biological Macromolecules. 2019; 122:1035-1045.
36. Deng A, Kang X, Zhang J, Yang Y, Yang S: Enhanced gelation of chitosan/beta-sodium glycerophosphate thermosensitive hydrogel with sodium bicarbonate and biocompatibility evaluated. Materials Science and Engineering C: Materials for Biological Applications. 2017; 78:1147-1154.
37. Xiao B, Zhang Z, Viennois E, Kang Y, Zhang M, Han MK, Chen J, Merlin D: Combination Therapy for Ulcerative Colitis: Orally Targeted Nanoparticles Prevent Mucosal Damage and Relieve Inflammation. Theranostics. 2016; 6:2250-2266.
38. Lee Y, Sugihara K, Gillilland MG, Jon S, Kamada N, Moon JJ: Hyaluronic acid-bilirubin nanomedicine for targeted modulation of dysregulated intestinal barrier, microbiome and immune responses in colitis. Nature materials. 2020; 19:118-126.
39. Madhusudanan P, Raju G, Shankarappa S: Hydrogel systems and their role in neural tissue engineering. Journal of the Royal Society Interface. 2020; 17:20190505.
40. Shi J, Xie Q, Yue Y, Chen Q, Zhao L, Evivie SE, Li B, Huo G: Gut microbiota modulation and anti-inflammatory properties of mixed lactobacilli in dextran sodium sulfate-induced colitis in mice. Food Function. 2021; 12:5130-5143.
41. Zhang J, Zhao Y, Hou T, Zeng H, Kalambhe D, Wang B, Sheng X, Huang Y: Macrophage-based nanotherapeutic strategies in ulcerative colitis. Journal of Controlled Release. 2020; 320:363-380.
42. Jeon Y-D, Lee J-H, Lee Y-M, Kim D-K: Puerarin inhibits inflammation and oxidative stress in dextran sulfate sodium-induced colitis mice model. Biomedicine & Pharmacotherapy. 2020; 124:109847.

Figures

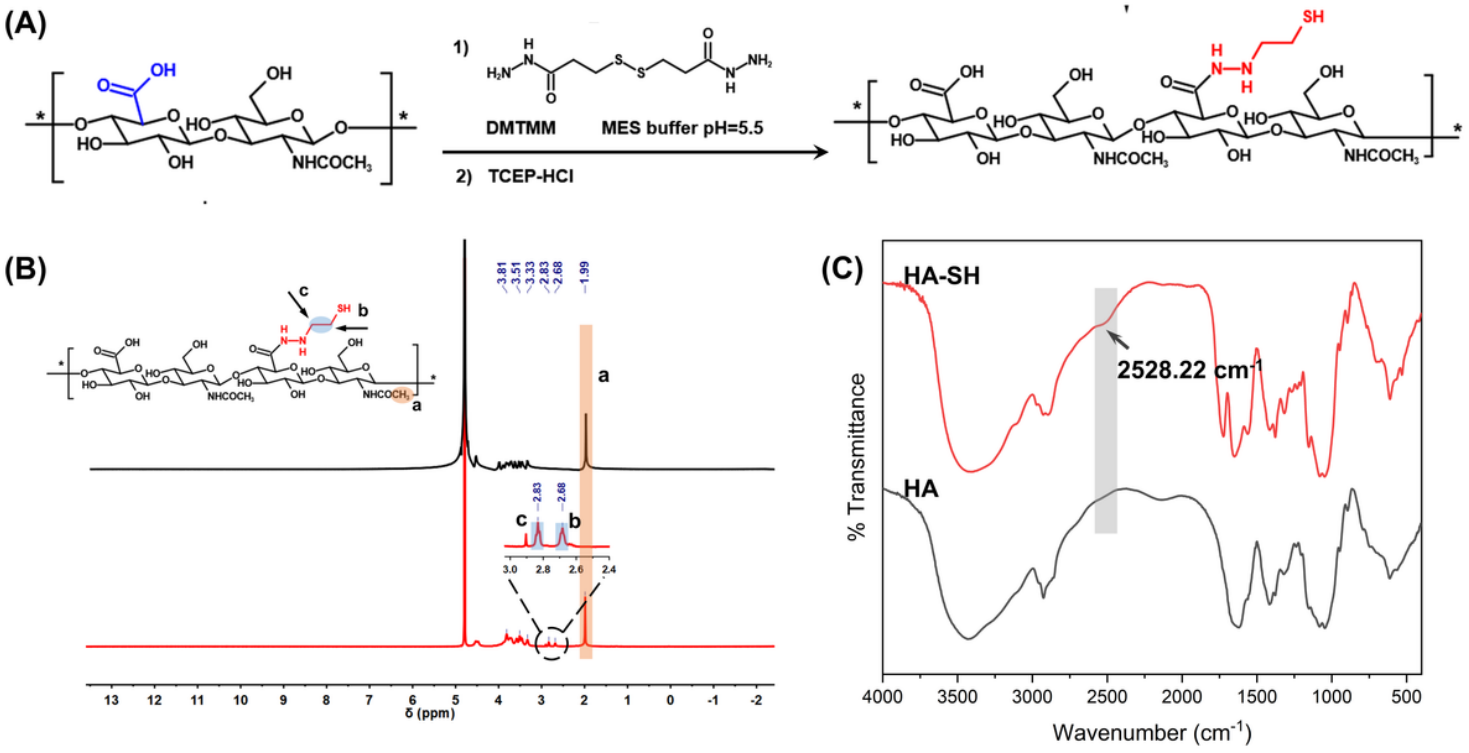

Figure 1

Synthesis and characterization of HA-SH. (A) The synthetic route of HA-SH, (B) ^{1}H NMR of HA and HA-SH, (C) FT-IR of HA and HA-SH.

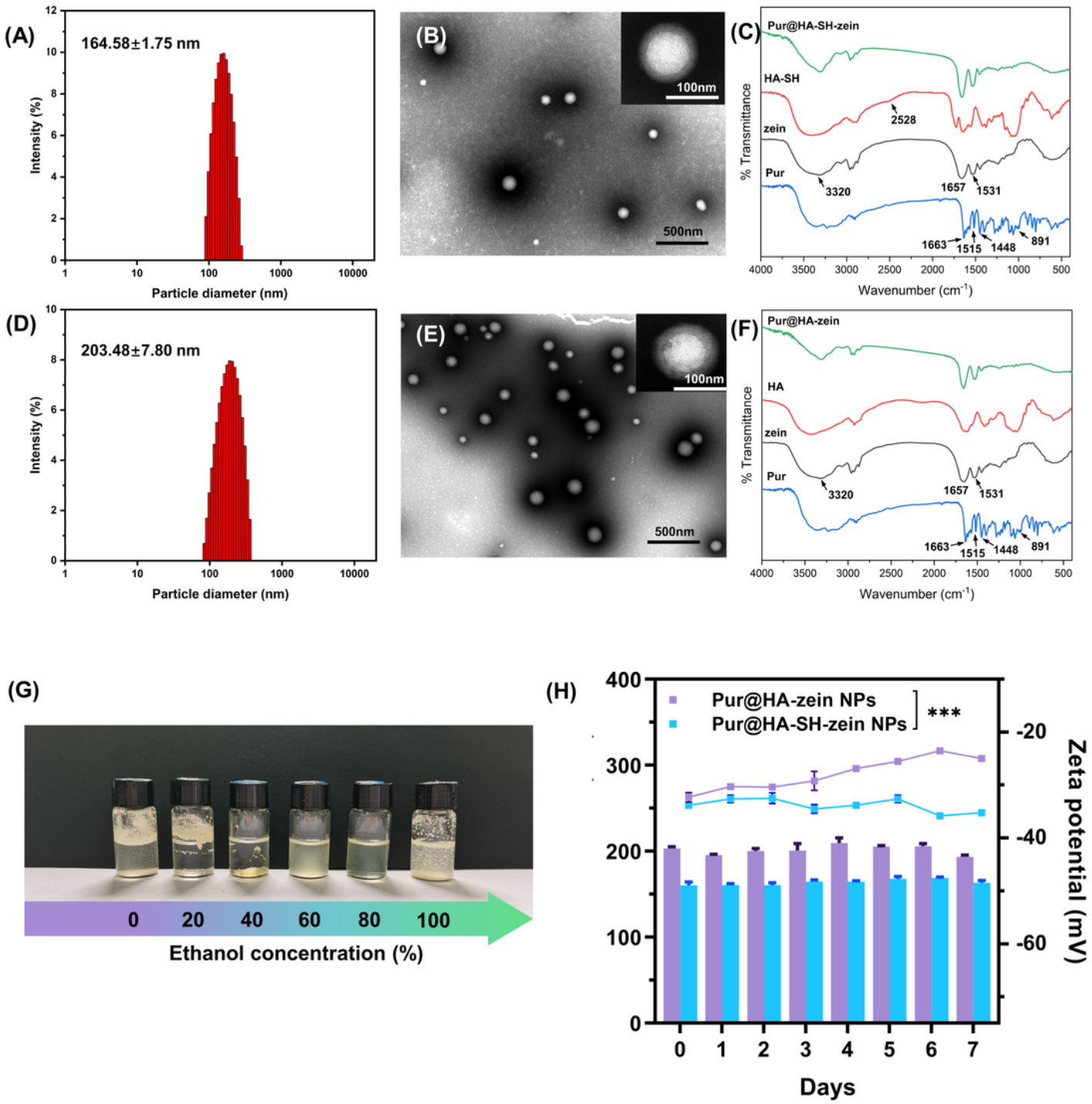

Figure 2

Characterization of Pur@HA -zein NPs and Pur@HA-SH-zein NPs. (A) Particle size distribution of Pur@HA-zein NPs, (B) TEM of Pur@HA-zeinNPs, (C) FT-IR of Pur, zein, HA and Pur@HA-zeinNPs, (D) Particle size distribution of Pur@HA-SH-zein NPs, (E) TEM of Pur@HA-SH-zein NPs, (F) FT-IR of Pur, zein, HA-SH and Pur@HA-SH-zeinNPs, (G) Solubility of zein in different concentrations of ethanol, (H) Stability within 7 days of Pur@HA-zein NPs and Pur@HA-SH-zein NPs.

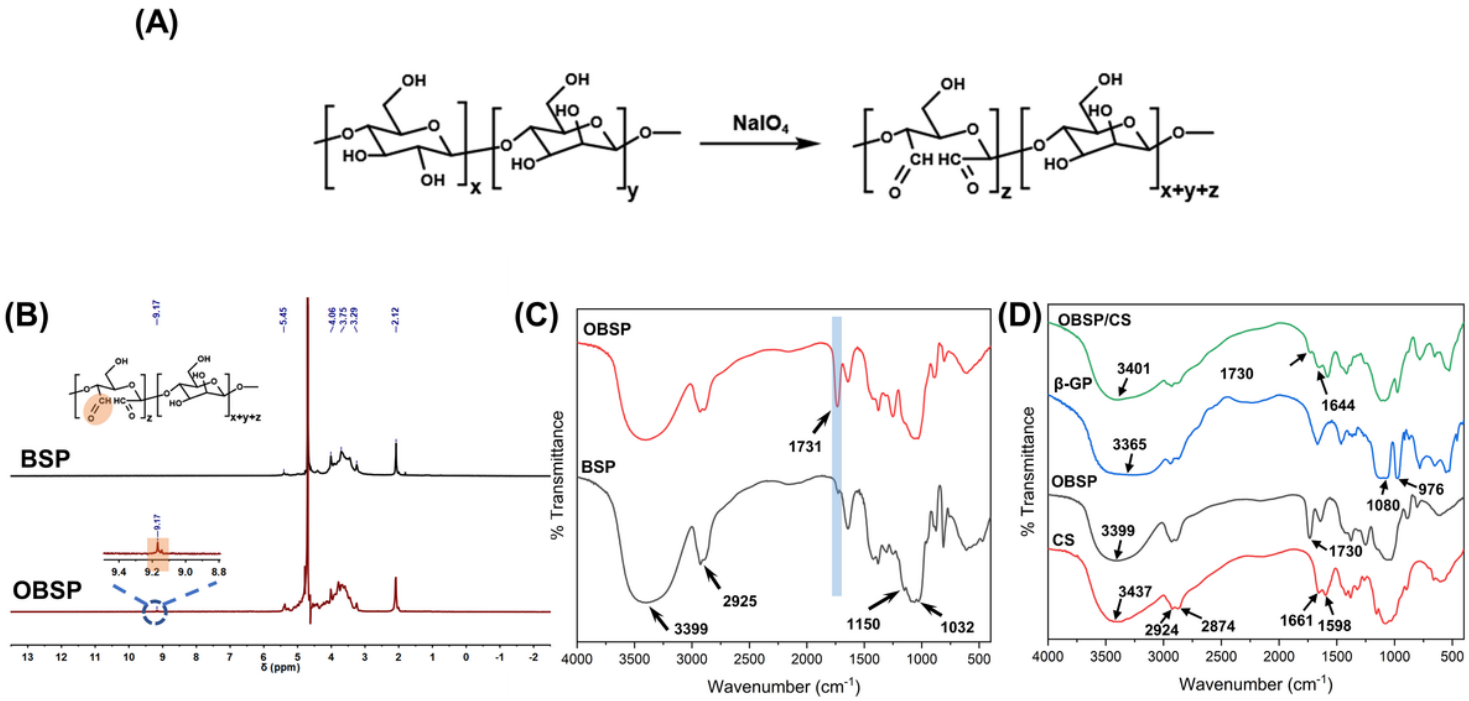

Figure 3

Characterization of OBSP and OBSP/CS hydrogel. (A) The synthetic route of OBSP, (B) ^{1}H NMR of BSP and OBSP, (C) FT-IR of BSP and OBSP, (D) FT-IR of CS, OBSP, β-GP and OBSP/CS.

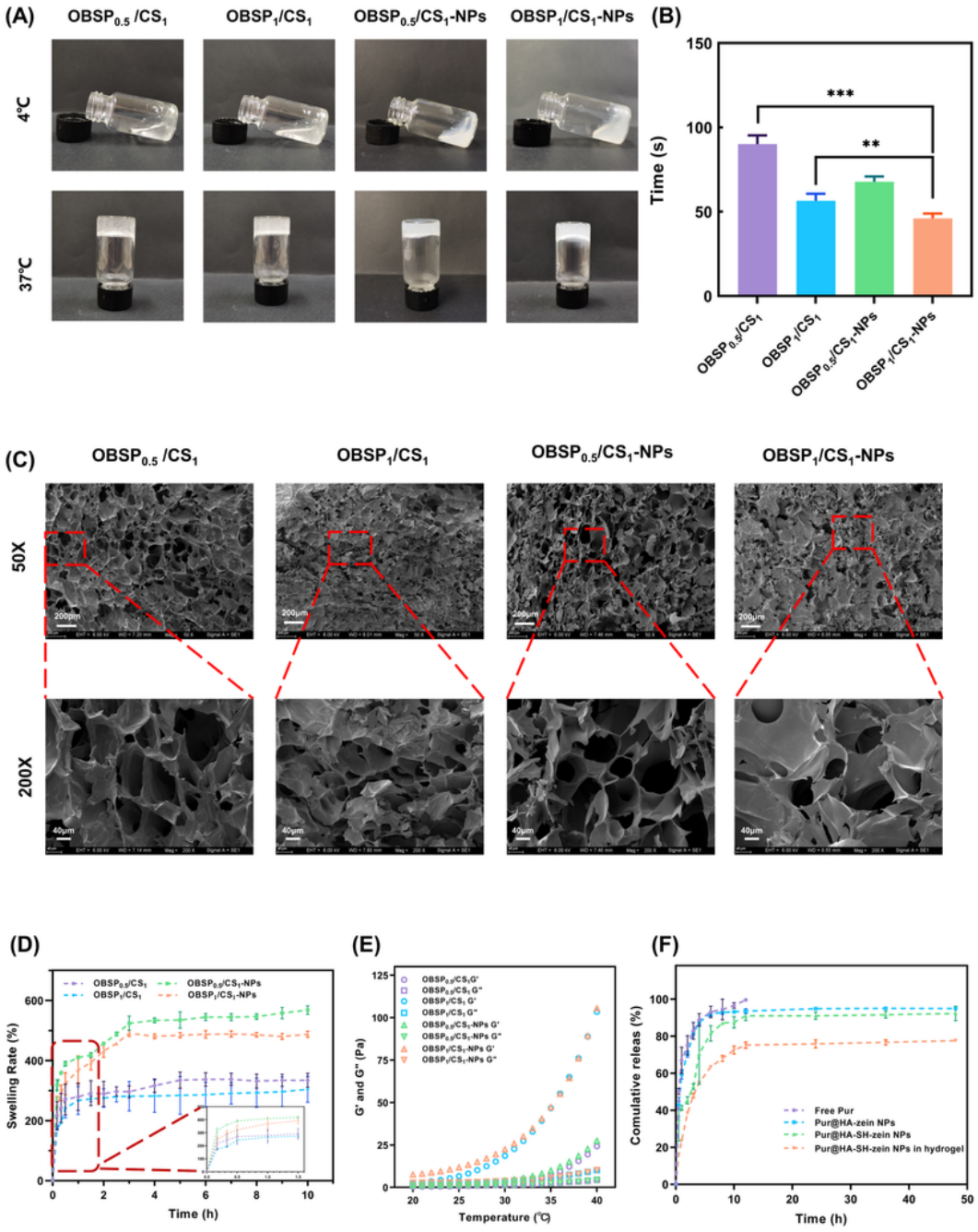

Figure 4

Characterization of four thermosensitive hydrogels. (A) Temperature response of different hydrogel groups, (B) Gelation time of different thermosensitive hydrogel groups (n=5), (C) SEM images of different thermosensitive hydrogel groups, (D) Swelling rate of hydrogels, (E) The rheological properties of different thermosensitive hydrogel groups (n=3), (F) Release of Pur in free Pur, Pur@HA-zein NPs,

Pur@HA-SH-zein NPs and Pur@HA-SH-zein NPs in Hydrogel *in vitro* (n = 3). The data are displayed as the mean ± standard deviation (SD).

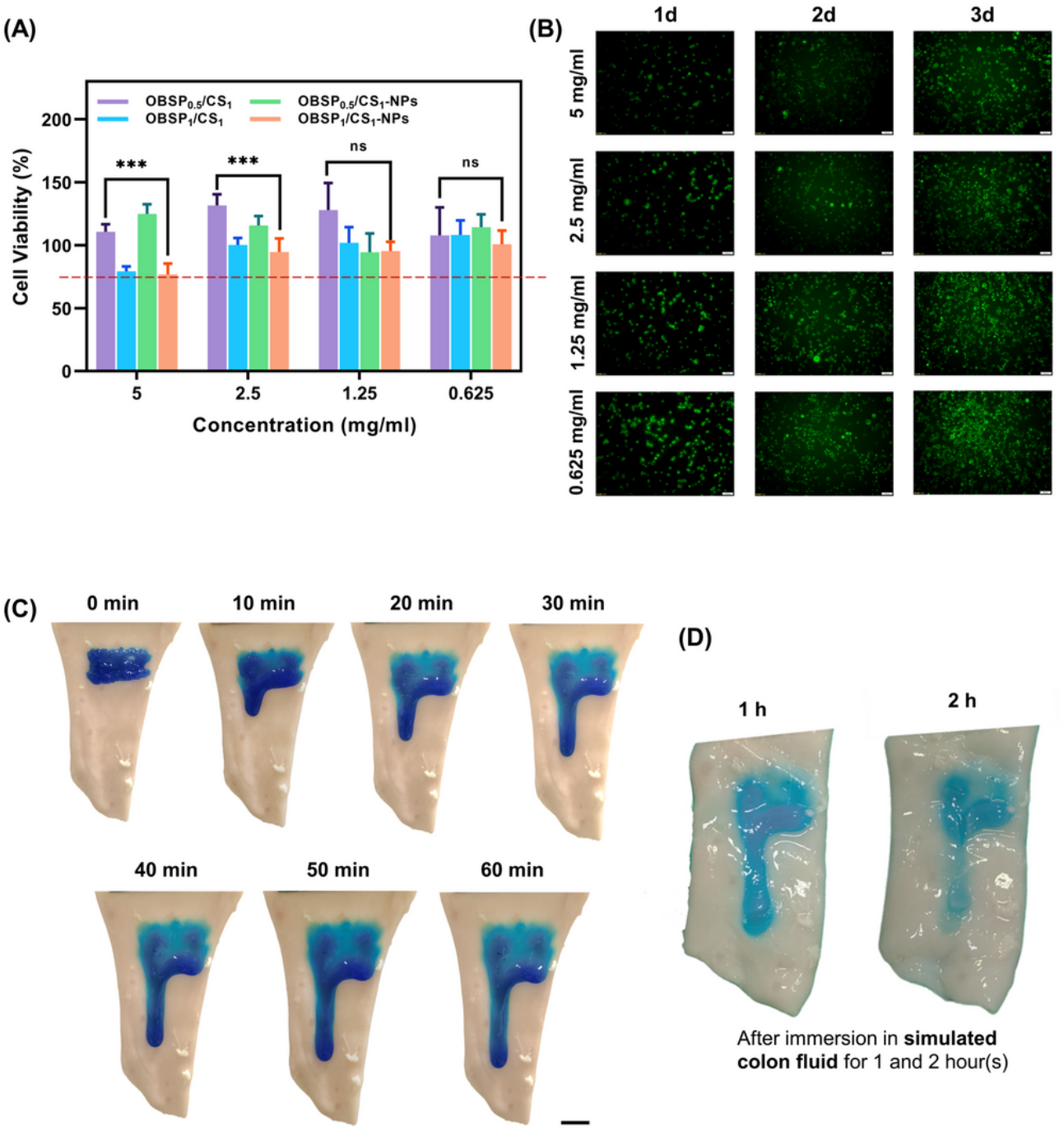

Figure 5

Biocompatibility and adhesion in vitro. (A) *In vitro* biocompatibility of different hydrogel groups on L929 Mouse fibroblast cells (n=6), (B) Cell proliferation in 3d of Pur@HA-SH-zein NPs in Hydrogel, (C-D) The *in*

*vitro*adhesion of MB@HA-SH-zein NPs in Hydrogel (Scale bar: 1 cm).

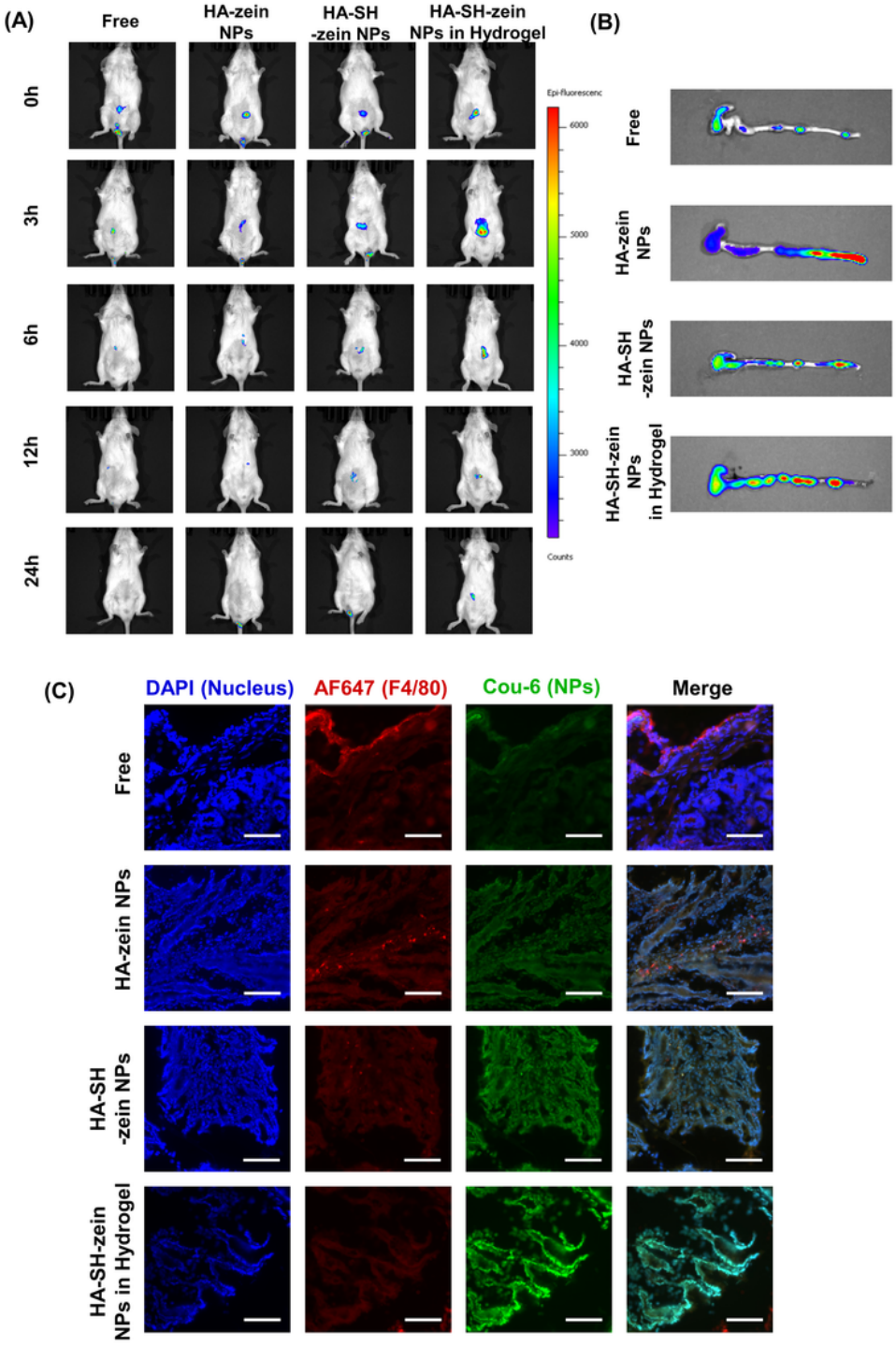

Figure 6

Retention, distribution, and permeation *in vivo*. (A) Fluorescence images of UC mice after rectal administration of free IR780, IR780@HA-zein NPs, IR780@HA-SH-zein NPs and IR780@HA-SH-zein NPs in Hydrogel at 0, 3, 6, 12, and 24 h, (B) Fluorescence images of the colon tract after rectal administration of

free IR780, IR780@HA-zein NPs, IR780@HA-SH-zein NPs and IR780@HA-SH-zein NPs in Hydrogel at 24 h, (C) Immunofluorescence images of the UC tissues after rectal delivery of free C6, C6@HA-zein NPs, C6@HA-SH-zein NPs and C6@HA-SH-zein NPs in Hydrogel at 24 h (Scale bar: 100 μm).

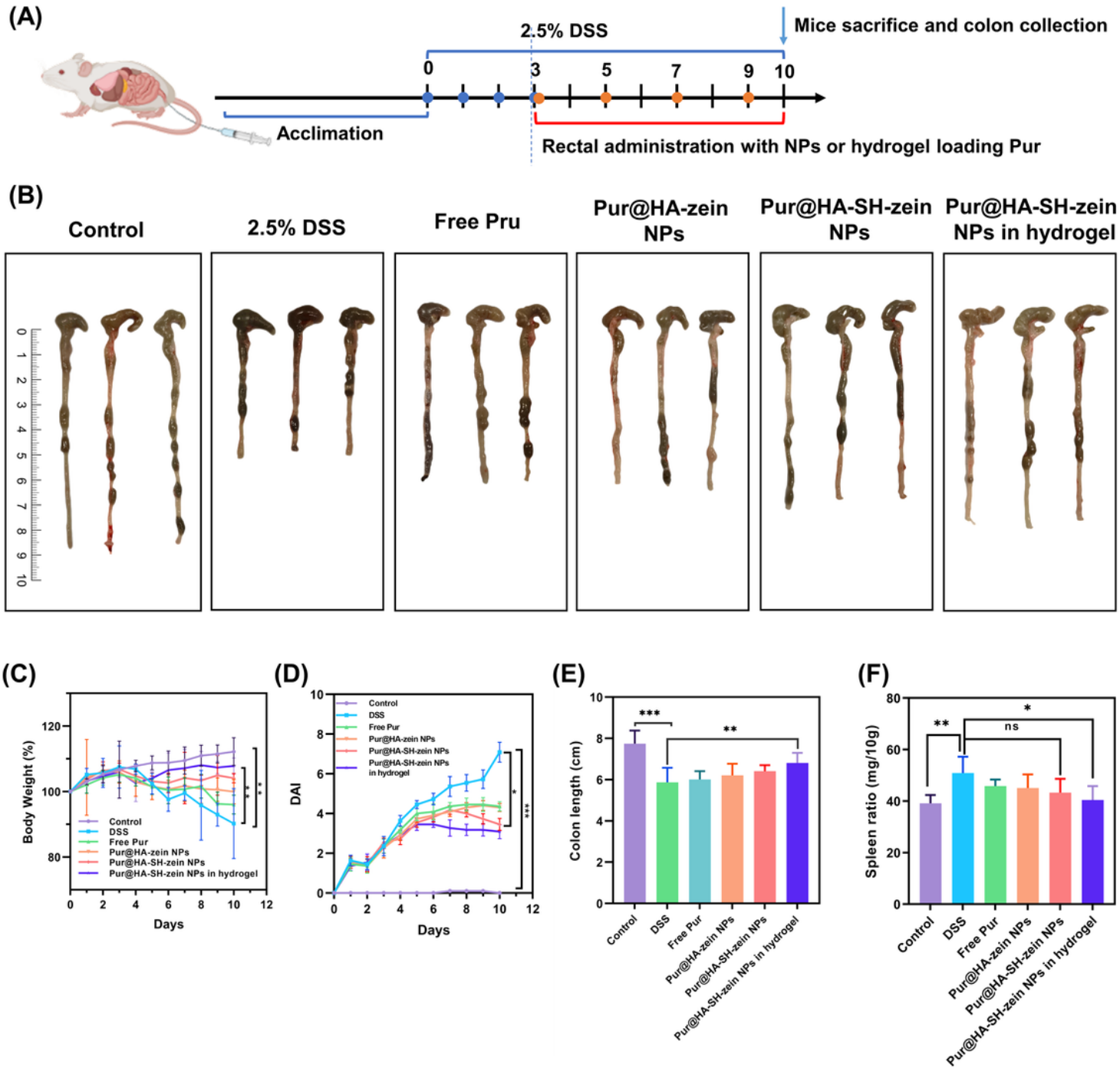

Figure 7

In vivo therapeutic effect of thermosensitive hydrogel against UC. (A) Illustration of the experimental protocol, (B) Photographs of murine colon after rectal administration with different Pur preparations, (C) Body weight of mice among different Pur preparation, (D) DAI of mice among different Pur preparation, (E) Colon length of mice among different Pur preparation, (F) Spleen ratio of mice among different Pur preparation. The data are displayed as the mean ± SD (n=6; *p < 0.05, **p < 0.01, ***p < 0.001; and n.s. means no significant difference.)

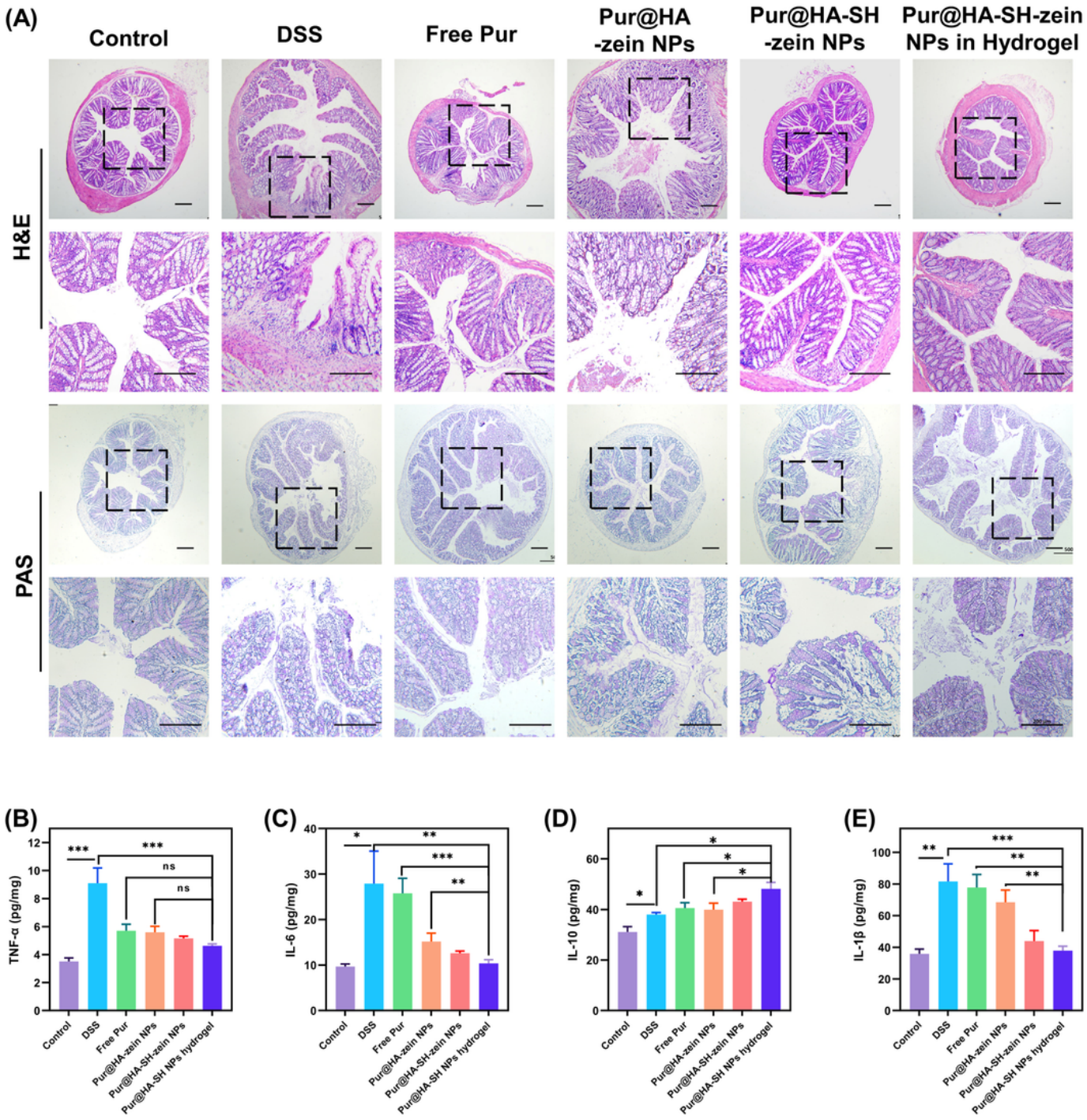

Figure 8

Expression of H&E and PAS staining and inflammatory factors in colon tissues. (A) H&E and PAS staining (Scale bar: 200 μm), (B-E) Inflammatory factors including TNF-α, IL-6, IL-10 and IL-1β. The data are displayed as the mean ± SD (n=6; *p < 0.05, **p < 0.01, ***p < 0.001; and n.s. means no significant difference.)

Supplementary Files

This is a list of supplementary files associated with this preprint. Click to download.

- GraphicalAbstract.png
- SupplementaryMaterial.docx